

1 **Mapping quantal touch using 7 Tesla functional magnetic resonance imaging**  
2 **and single-unit intraneural microstimulation**

3

4

5 Sanchez Panchuelo RM<sup>1\*</sup>, Ackerley R<sup>2,3\*</sup>, Glover PM<sup>1</sup>, Bowtell RW<sup>1</sup>, Wessberg J<sup>2</sup>,  
6 Francis ST<sup>1§</sup> and McGlone F<sup>4§</sup>

7

8 \* These authors contributed equally to this work.

9 § These authors contributed equally to this work.

10

11 <sup>1</sup>Sir Peter Mansfield Imaging Centre, School of Physics and Astronomy, University of  
12 Nottingham, Nottingham, NG7 2RD, UK

13 <sup>2</sup>Department of Physiology, University of Gothenburg, Göteborg, SE-405 30,  
14 Sweden.

15 <sup>3</sup>Laboratoire de Neurosciences Intégratives et Adaptatives (UMR 7260), Aix-  
16 Marseille Université – CNRS, Marseille, France

17 <sup>4</sup>School of Natural Sciences and Psychology, Liverpool John Moores University,  
18 Liverpool, L3 3AF, UK

19

20 Corresponding author: Rosa Sanchez Panchuelo

21 Email: [rosa.panchuelo@nottingham.ac.uk](mailto:rosa.panchuelo@nottingham.ac.uk)

22

23

24 Key words: touch, microneurography, intraneural microstimulation, peripheral nerves,  
25 hand, tactile, fMRI, ultra-high field

26

27

28 **Abstract**

29 Using ultra-high field 7 Tesla (7T) functional magnetic resonance imaging (fMRI), we  
30 map the cortical and perceptual responses elicited by intraneural microstimulation  
31 (INMS) of single mechanoreceptive afferent units in the median nerve, in humans.  
32 Activations are compared to those produced by applying vibrotactile stimulation to  
33 the unit's receptive field, and unit-type perceptual reports are analyzed. We show that  
34 INMS and vibrotactile stimulation engage overlapping areas within the  
35 topographically appropriate digit representation in the primary somatosensory cortex.  
36 Additional brain regions in bilateral secondary somatosensory cortex, premotor  
37 cortex, primary motor cortex, insula and posterior parietal cortex, as well as in  
38 contralateral prefrontal cortex are also shown to be activated in response to INMS.  
39 The combination of INMS and 7T fMRI opens up an unprecedented opportunity to  
40 bridge the gap between first-order mechanoreceptive afferent input codes and their  
41 spatial, dynamic and perceptual representations in human cortex.

## 42 INTRODUCTION

43 The primary somatosensory cortex (S1) has been extensively explored in animal  
44 studies where it has been shown that this area displays multiple, fine-grained  
45 representations of the body (Paul et al. 1972; Kaas et al. 1979; Favorov et al. 1987).  
46 Penfield and Boldrey (Penfield & Boldrey 1937) derived the first maps of the  
47 somatotopic human body representation in S1 using electrical stimulation of the  
48 cortical surface. Somatosensory research in humans has involved using  
49 psychophysical (Klatzky et al. 1985; Gescheider et al. 2002), microneurographic  
50 (Vallbo & Johansson 1984; Johansson & Vallbo 1983), and neuroimaging (McGlone  
51 et al. 2002; Martuzzi et al. 2014; Servos et al. 2001) techniques to study different  
52 stages and levels of detail in somatosensory function. Functional magnetic  
53 resonance imaging (fMRI) has been used extensively for non-invasive study of the  
54 somatosensory cortices in humans (Nelson & Chen 2008; McGlone et al. 2002;  
55 Sanchez-Panchuelo et al. 2010). Most such fMRI studies have investigated the  
56 spatial pattern of cortical activation in response to vibrotactile (Francis et al. 2000;  
57 Sanchez-Panchuelo et al. 2010) or pneumatic (Huang & Sereno 2007; Overduin &  
58 Servos 2008) mechanical stimulation of the digits, or to electrical stimulation of the  
59 skin (Blankenburg et al. 2003) or median nerve (Kampe et al. 2000; Ferretti et al.  
60 2007). These approaches excite large populations of different classes of  
61 mechanoreceptive afferents resulting in relatively diffuse activations in contralateral  
62 S1 and bilateral secondary somatosensory cortex (S2).

63         Microneurography provides a method to record the spike discharge activity of  
64 a single mechanoreceptive afferent in conscious humans (Vallbo & Hagbarth 1968)  
65 to determine its response to skin contact and the properties of its receptive field, i.e.  
66 location, size, and shape. In this manner, mechanoreceptive afferents innervating the  
67 glabrous skin of the hand can be categorized into one of four types: fast-adapting  
68 type 1 (FA1), fast-adapting type 2 (FA2), slowly-adapting type 1 (SA1), and slowly-  
69 adapting type 2 (SA2) (Vallbo & Johansson 1984). In intraneural microstimulation

70 (INMS), single mechanoreceptive afferents are selectively activated by passing a  
71 small (1-7  $\mu$ A) current through the recording microelectrode, thus evoking a quantal  
72 sensation in the projected sensory field, which matches the physiological qualities of  
73 the recorded mechanoreceptive afferent (Torebjörk et al. 1987). Microstimulation of  
74 an FA1 afferent evokes a well-defined, local sensation of 'flutter' or 'buzzing', while  
75 microstimulation of an SA1 afferent evokes a sensation of continuous pressure or  
76 inward pulling (Vallbo et al. 1984; Ochoa & Torebjörk 1983). Microstimulation of an  
77 FA2 afferent evokes a diffuse sensation of vibration over a larger area, whereas  
78 microstimulation of an SA2 afferent does not produce a consistent, conscious  
79 sensory experience (Vallbo et al. 1984; Ochoa & Torebjörk 1983).

80 It has been shown in a small number of previous studies that INMS of single  
81 mechanoreceptive afferents can be combined with noninvasive imaging methods to  
82 advance our understanding of the effects of mechanoreceptive afferent activity in  
83 somatosensory cortices. For example, INMS of FA1 and SA1 afferents in the median  
84 nerve produces frequency-following electroencephalography responses within  
85 contralateral S1 (Kelly et al. 1997). The single previous study combining INMS with  
86 fMRI (Trulsson et al. 2001), using a 3 T scanner and a surface coil positioned over  
87 the parietal lobe contralateral to the site of stimulation, showed that INMS of FA1 and  
88 SA1 afferents induced activity in S1 and S2, which overlapped with regions activated  
89 by applying mechanical vibration to the relevant units' receptive fields. However, a  
90 detailed characterization of the specificity of single unit INMS activations within the  
91 representation of the digits in S1 has yet to be performed.

92 Several studies have previously assessed the cortical response to vibrotactile  
93 stimulation of the glabrous skin of the human hand, and shown that this evokes a  
94 hemodynamic response in multiple primary and secondary cortical areas, including  
95 contralateral S1, bilateral S2, primary motor cortex (M1), supplementary motor area  
96 (SMA), cingulate cortex, posterior parietal cortex (PPC), and insula cortex (McGlone  
97 et al. 2002; Trulsson et al. 2001; Gelnar et al. 1998). Ultra-high field (7T) fMRI has

98 also recently been used in conjunction with vibrotactile stimulation to map individual  
99 digit representations and resolve the fine, within-digit organization (base-to-tip), thus  
100 revealing functional subdivisions of areas in S1 (Sanchez-Panchuelo et al. 2010;  
101 Sanchez-Panchuelo et al. 2012). Compared to lower field measurements, 7T fMRI  
102 provides greatly increased sensitivity and blood-oxygenation level dependent (BOLD)  
103 signal contrast, coupled with improved intrinsic spatial specificity (Gati et al. 1997).  
104 Here, we used 7T fMRI to resolve whole-brain cortical activation patterns evoked by  
105 INMS of single mechanoreceptive afferent units in the glabrous skin of the hand, and  
106 to assess the precise spatial localization of INMS-evoked BOLD responses in  
107 contralateral S1, in comparison to activation due to mechanical vibrotactile  
108 stimulation.

109

## 110 **RESULTS**

111 Recordings were made from 28 mechanoreceptive afferents (17 FA1, 14 SA1, 1 FA2  
112 and 1 SA2) in 4 participants during 10 experimental sessions. We focused our study  
113 on the cortical response to stimulation of type 1 afferents (FA1 and SA1), as these  
114 units are far more numerous in the volar hand than type 2 units (FA2 and SA2)  
115 (Vallbo & Johansson 1984). Example recordings from FA1 and SA1 units are shown  
116 in Figures 1a and 1b respectively, demonstrating that good quality signals can be  
117 recorded from single mechanoreceptive afferents in the environment of a 7T  
118 magnetic resonance scanner. INMS of single units produced distinct sensations: FA1  
119 stimulation was typically felt as vibration or buzzing, while SA1 stimulation elicited a  
120 sensation of pressure or pulling (see Table 1).

121         Due to the technically challenging set-up (e.g. 2 units were lost on moving the  
122 participant into the scanner bore) and the nature of the method (e.g. the stimulated  
123 unit corresponds to the unit from which recordings were previously made only around  
124 50 % of the time (Torebjörk et al. 1987)), INMS was carried out during concurrent  
125 fMRI in 11 units (U1-U11) that gave single-point sensations, 6 of which were

126 electrophysiologically-characterized (see Table 1). The receptive field locations for  
127 these units are shown in Figure 1c.

128

129 **Cortical responses to single unit INMS and vibrotactile stimulation in S1:** Clear  
130 and reproducible BOLD responses were found in somatosensory regions, when  
131 INMS was perceived. Occasionally, participants reported that the sensation evoked  
132 by the INMS stopped, likely due to a minor dislodgement of the microelectrode. This  
133 occurred for U7 where a projected sensation was perceived prior to scanning, but no  
134 sensation was felt during the fMRI run. For some units, the sensation was weak (U2,  
135 U3; possibly due to difficulty in attending to the stimulus sensation when inside the  
136 scanner), or lost during the fMRI run (U5, U6, U8). We compared the location of fMRI  
137 responses of all perceived INMS units in contralateral S1 with the digit representation  
138 obtained from both vibrotactile stimulation of the microstimulated unit's receptive field  
139 and the fMRI somatotopy maps formed from the traveling-wave (phase-encoding)  
140 vibrotactile paradigm (Figure 2). We found that fMRI responses to INMS of single  
141 units (all except for U1; Figure 3. – figure supplement 1) were spatially localized  
142 within the relevant S1 digit representation identified from vibrotactile stimulation.  
143 Figure 2a shows example maps of digit somatotopy defined from the vibrotactile  
144 traveling-wave paradigm for Participant 4 in the right and left hemispheres (left and  
145 right of the figure, respectively). Figure 2b shows the BOLD response to INMS of U11  
146 (right) and U9 (left) for Participant 4. These responses are well-localized within  
147 regions of the somatotopic map for digit 4 of the left hand and digit 1 of the right  
148 hand, respectively. Figure 2c shows the activation generated in S1 by applying  
149 vibrotactile stimulation to the receptive field of U11 (right) and U9 (left). Fits to the  
150 hemodynamic responses evoked in S1 by INMS and the application of vibrotactile  
151 stimulation to the unit's receptive field can be seen in Figure 2d.

152 Figure 3 shows the spatial localization of the activation produced in S1 by the  
153 seven perceived INMS units (U4-U6, U8-U11) (Figure 3a) and corresponding

154 vibrotactile stimulation of each units' receptive field (Figure 3b). In general, the BOLD  
155 responses due to INMS and vibrotactile stimulation were well localized within the  
156 expected digit ROI, as defined from the traveling-wave somatotopy paradigm. Figure  
157 3c plots the average INMS z-score (FDR corrected) in each digit ROI, and Figure 3d  
158 shows the proportion of active voxels to the INMS paradigm that were classified to  
159 each digit ROI ( $z > 3.08$ , FDR corrected). As expected, the average z-score and  
160 proportion of active voxels in the digit ROIs corresponding to digits in which the INMS  
161 was sensed was higher than in the neighboring digits. Figure 4 plots the group-level  
162 response to show the spatial spread of the INMS and vibrotactile response to  
163 neighboring digits. Figure 4a shows the mean z-score, Figure 4b the proportion of  
164 active voxels and Figure 4c the GLM parameter estimate to INMS (top) and  
165 vibrotactile stimulation of the unit's receptive field (bottom). ANOVA results showed a  
166 significant difference in mean Z-score ( $F_{4,30}=14.08$ ,  $P < 10^{-5}$ ;  $F_{4,30}=12.97$ ,  $P < 10^{-5}$ ),  
167 proportion of active voxels ( $F_{4,30}=16.12$ ,  $P < 10^{-6}$ ;  $F_{4,30}=17.64$ ,  $P < 10^{-6}$ ) and GLM  
168 parameter estimates ( $F_{4,30}=13.52$ ,  $P < 10^{-5}$ ;  $F_{4,30}=14.1$ ,  $P < 10^{-5}$ ) across the stimulated  
169 and neighboring digit classification (INMS; vibrotactile). A multiple pairwise  
170 comparison, adjusted for multiple comparisons, showed that measures for the  
171 stimulated digit were significantly higher than those of the neighboring digits for mean  
172 Z-score ( $P < 0.0001$  INMS;  $P < 0.005$  vibrotactile stimulation), proportion of active  
173 voxels ( $P < 0.00005$  for INMS and vibrotactile stimulation) and GLM parameter  
174 estimates ( $P < 0.01$  for INMS and vibrotactile stimulation).

175         For those units lost during the fMRI run (U5, U6, U8), no areas were found to  
176 show a significant correlation with an additional (parametric) regressor when  
177 modelling linear reductions in induced response over time (to model gradual losses  
178 of unit responses), likely due to the sudden rather than gradual loss of the unit. Thus  
179 parameter estimates to INMS stimulation were not significantly different between the  
180 GLM including a parametric regressor and the modelling INMS stimulation alone.

181

182 **Comparison of cortical activity patterns between single unit INMS and**  
183 **vibrotactile stimulation:** Participants freely described the mechanical, point-  
184 vibrotactile stimulus applied to each unit's receptive field as feeling very similar in  
185 extent and quality to the INMS, especially for the sensations generated from FA1  
186 units. Figure 5a compares the of mapping INMS-induced fMRI responses (yellow) for  
187 all FA1 single units to maps of the responses produced by applying vibrotactile  
188 stimulation to the units' receptive fields (blue). Overlapping cortical responses are  
189 shown in green. Activation maps show the conjunction of the individual FA1 unit  
190 responses, using the same statistical threshold ( $Z > 3.08$ , false discovery rate (FDR)  
191 correction) for both INMS and vibrotactile stimulation. BOLD responses to single unit  
192 INMS were detected in a number of sensory-related brain areas, including S1, S2  
193 (Brodmann areas (BA) 40 and 43), premotor cortex (PMC; SMA and dorsal PMC),  
194 M1, insula (anterior insula cortex (AIC) and posterior insula cortex (PIC)), prefrontal  
195 cortex (PFC) and PPC. Table 2 details the location and statistical significance (mean  
196 and standard error across units) of the BOLD responses produced in these areas by  
197 INMS of the five FA1 single units in the left hand. Common areas of activation for  
198 INMS and vibrotactile stimulation included S1, S2, PMC, M1, and contralateral PIC;  
199 however, INMS gave rise to significant activity in additional brain regions, including  
200 the AIC, PPC and contralateral PFC (Table 2). Figure 5b shows that the HRFs  
201 generated in these regions by INMS were similar in both onset and duration to the  
202 INMS-elicited responses in S1 and S2.

203

## 204 **DISCUSSION**

205 The principal finding of our present work is the detailed localization in contralateral  
206 S1 of cortical responses to the electrical microstimulation of single, first-order  
207 mechanoreceptive afferents, and the demonstration of spatial alignment of these  
208 responses with somatotopic maps derived from mechanical skin stimulation. This  
209 was achieved through the combined usage of two techniques: intra-neural



210 microstimulation (INMS), to stimulate single mechanoreceptive afferents, and 7T  
211 fMRI, to map the cortex with superior spatial resolution. This work also shows that  
212 activity generated by stimulation of a single mechanoreceptive afferent can be  
213 perceptually characterized and produces a network of cortical responses.

214         Only one previous study has combined single unit INMS with fMRI, at 3T  
215 (Trulsson et al. 2001), but this was only able to resolve activation in contralateral S1  
216 and S2 as the use of a surface coil limited the spatial extent of activation maps. The  
217 greater signal-to-noise ratio and improved BOLD contrast afforded by 7T fMRI  
218 allowed us to improve the spatial resolution, with a reduction in the voxel volume by a  
219 factor of 6 compared to previous work at 3T (Trulsson et al. 2001). We have  
220 exploited the improved spatial resolution to provide a detailed characterization of the  
221 location and extent of the cortical network involved in encoding inputs from single  
222 mechanoreceptive afferents, as well as in comparing these responses to  
223 somatotopical maps created from vibrotactile skin stimulation.

224         Measurements of cortical activity elicited by INMS demonstrated that when a  
225 singular, quantal touch from the stimulation of a single mechanoreceptive afferent is  
226 consciously felt, a precise area in contralateral S1 is active. The response in S1 was  
227 well-localized within the expected region, identified from maps of digit somatopy  
228 obtained from vibrotactile stimulation of the fingertips. The extent of the S1  
229 responses to INMS was less than that elicited by vibrotactile stimulation to the unit's  
230 receptive field, although the response produced by single unit INMS was relatively  
231 extensive, considering that vibrotactile stimulation simultaneously engages a large  
232 number of afferents (Johansson & Vallbo 1979; Vallbo & Johansson 1984).

233         Robust responses were found within the expected digital cortical area for all  
234 perceived microstimulated afferents (Figures 2 and 3), except for U1, for which no  
235 significant responses were found, in either contralateral or ipsilateral S1, despite the  
236 fact that the participant exhibited a complete somatotopic map of the digits in both  
237 hemispheres and reported feeling the sensation throughout INMS. To explore this

238 finding further, we used the delineation of digits 2 and 3 from the somatotopic map  
239 obtained with the vibrotactile traveling-wave paradigm to inspect the time series of S1  
240 responses evoked by INMS for U1 (located on the palm below digit 2). We also  
241 interrogated the BOLD response produced in contralateral S1 when vibrotactile  
242 stimulation was applied to the receptive fields of U1. In S1, we found negative BOLD  
243 responses (Figure 3 – figure supplement 1) for both INMS and vibrotactile stimulation  
244 applied to the receptive field of the INMS. The negative BOLD response in this  
245 subject is possibly due to a steal effect from the nearby vasculature draining from the  
246 active cortex (Bianciardi et al. 2011) since draining venous regions are highly  
247 modulated by block paradigms with periods of 'on' and 'off' stimulation, as used to  
248 study the response to INMS and vibrotactile stimulation of the receptive field. In  
249 contrast, using the traveling-wave paradigm a complete map of the digits in S1 is  
250 seen. This is expected, as we have previously shown that a traveling-wave design is  
251 insensitive to the non-specific BOLD contributions from large veins that drain blood  
252 from across the whole hand representation in S1 (Uğurbil et al. 2003; Besle et al.  
253 2013), thus suppressing the venous signal modulations found in the block  
254 INMS/vibrotactile stimulation data. In order to estimate the spatial spread of INMS  
255 BOLD responses to neighboring digits, we show that, at the group level, the z-score,  
256 proportion of active voxels and GLM parameter estimates are significantly higher  
257 ( $p < 0.01$ ) in the stimulated ROI than in the neighboring digits (Figure 4). These results  
258 are in-line with our previous findings reported for vibrotactile stimulation (Besle 2013).

259         The network of cortical areas activated by both INMS of single  
260 mechanoreceptive afferents and mechanical vibrotactile stimulation of the units'  
261 receptive field, included somatosensory areas such as S1, S2, and PIC, as well as  
262 areas involved in motor control, including M1, SMA and PMC. Although M1 has  
263 previously been shown to be activated by tactile input (e.g. Francis et al. 2000;  
264 Ackerley et al. 2012), we cannot exclude the possibility that the M1 activation  
265 observed in this study may originate from spatial blurring of somatosensory activation

266 (given that M1 and S1 are located on opposite banks of the central sulcus). When  
267 comparing responses to INMS and vibrotactile stimulation applied to the afferents'  
268 receptive fields, INMS activated a number of additional areas, specifically the AIC,  
269 PPC and PFC. Exploration of the INMS BOLD time series for these areas (Figure 5b)  
270 suggests that the activity in these areas is locked to the S1/S2 activity and is not due  
271 to anticipation. Both insula and parietal cortices have been shown to contribute to the  
272 perception of touch (Preusser et al. 2014), and a previous study of tactile attention  
273 (Burton et al. 2008) has shown that a fronto-parietal network, which includes PFC  
274 and PPC, is involved in attention. Although identical paradigm timings were used for  
275 INMS and vibrotactile stimulation in order to compare the spatial localization of the  
276 BOLD response, there were differences in the attentional focus between the INMS  
277 and vibrotactile tasks. During the INMS fMRI runs, participants were aware that  
278 perception might be lost and hence had to concentrate on the stimulus and report  
279 any lack of sensation at the end of the run. In contrast, the vibrotactile stimulus was  
280 delivered at a suprathreshold level and participants did not have to monitor that the  
281 sensation was still present during the vibrotactile fMRI run. Hence, the increased  
282 activity in AIC, PFC and PPC observed in the present study may reflect the increased  
283 attentional effects (i.e., baseline or gain effects on evoked responses) during the  
284 INMS protocol compared to vibrotactile stimulation. However, this is a preliminary  
285 finding and requires further investigation with larger sample sizes and more  
286 quantitative analysis to be corroborated.

287         The capability of combining INMS with 7T fMRI has the following theoretical  
288 implications for human somatosensory research. Although the notion that peripheral  
289 input from the skin is represented directly by four cytoarchitectonic areas (BA 3a, 3b,  
290 1 and 2) in S1, each containing an orderly somatotopic map of the body surface has  
291 been supported by findings from animal studies (Kaas et al. 1979; Paul et al. 1972;  
292 Favorov et al. 1987; Tommerdahl et al. 2010) and 7T fMRI in humans (Sanchez-  
293 Panchuelo et al. 2010; Sanchez-Panchuelo et al. 2012; Martuzzi et al. 2014), a

294 simple point-to-point topographical correspondence between skin surface and  
295 cortical representation does not hold. In reality, there is integration and processing  
296 through axonal synapsing in the dorsal column nuclei and thalamus prior to  
297 mechanoreceptive information entering the cerebral cortex. There appears to be a  
298 preserved transmission from single, mechanoreceptive second-order neurons in the  
299 dorsal column (Vickery et al. 1994). At the level of the thalamus, an axon of a single  
300 ventral posterolateral nucleus terminates over a fairly wide, roughly 0.5 mm, cortical  
301 territory (Rausell & Jones 1995), where many individual thalamocortical axons  
302 spread out in discrete patches over several millimeters of S1 (Landry et al. 1987).  
303 This spread corresponds well with our finding that the cortical activation from a single  
304 mechanoreceptive afferent extends over an area that is not dissimilar to the area  
305 activated by input from many afferents through point-vibrotactile stimulation. Also,  
306 neurons in S1 cortical columns have extensive lateral excitatory connections, not  
307 only with neighboring neurons, but also with neurons several millimeters away in the  
308 same cortical area (Burton & Fabri 1995). We have shown that single unit INMS  
309 produces bilateral somatosensory activation, as well as influencing motor areas and  
310 cognitive networks (e.g. PPC, PFC). Such a wide spreading of stimulus-evoked  
311 activity has been clearly documented in microelectrode recording studies (Reed et al.  
312 2010). Overall, the spatiotemporal pattern of S1 response to vibrotactile stimulation is  
313 far from simple and its functional significance remains to be unraveled.

314 Translational insights from *in vivo* neurophysiological studies in non-human  
315 primates have driven much of the theoretical understanding of cortical mechanisms  
316 that govern human tactile perception, but operative procedures, especially those  
317 which alter the neurochemistry of cortical synaptic transmission (Masamoto et al.  
318 2009), may confound relating such findings to normal functioning of the human brain.  
319 This demonstration of the feasibility of combining INMS with 7T fMRI opens up the  
320 possibility of a range of further neuroimaging studies that will allow interrogation of  
321 the precise anatomical and physiological properties of the fundamental encoding of

322 touch. These include systematic investigation of the sub-cortical (e.g. thalamic)  
323 responses and laminar-specific cortical responses to INMS of different  
324 mechanoreceptive afferent classes using a variety of electrical stimulation patterns.

325

## 326 **MATERIALS AND METHODS**

327 Ten experimental sessions were conducted on four right-handed participants (30-64  
328 years, 2 male). Procedures were approved by the University of Nottingham Medical  
329 School Ethics Committee and all participants gave full, written, informed consent.  
330 Due to the precision needed in performing INMS within the magnetic resonance  
331 scanner, participants were required to lie extremely still and feel relaxed; all  
332 participants were accustomed to the fMRI environment (two participants had  
333 participated in INMS experiments previously). Each experimental session involved  
334 three steps: (1) microneurography for the characterization of a single  
335 mechanoreceptive afferent (Vallbo & Hagbarth 1968); (2) assessment of the  
336 sensation to INMS; (3) concurrent INMS and fMRI. Participants subsequently took  
337 part in a second fMRI session in which vibrotactile stimulation was delivered.

338 Participants lay on the scanner bed with their arm (the left arm in all cases  
339 except one experiment on the right arm) immobilized using cushions. Survey,  
340 reference and  $B_0$ -map scans were acquired, and an image-based shimming  
341 approach (Sanchez-Panchuelo et al. 2010) used to minimize magnetic field  
342 inhomogeneity, with the optimized shim currents remaining fixed throughout the  
343 subsequent fMRI runs. The participant was moved out of the bore of the magnet to  
344 perform Steps (1) and (2).

345 **Microneurography:** In Step 1, the median nerve was accessed at the wrist in order  
346 to isolate single axonal responses from mechanoreceptive afferents in the volar  
347 hand, on which to perform INMS (Trulsson et al. 2001). A high-impedance (~300-500  
348 k $\Omega$ ), insulated, tungsten recording/stimulating electrode (15 mm length, shaft  
349 diameter 0.2 mm, tip diameter ~5  $\mu$ m; FHC, Bowdoin, ME) was inserted

350 percutaneously into the skin, ~3 cm from the wrist fold between the flexor carpi  
351 radialis and the flexor palmaris longus tendons. An uninsulated reference electrode  
352 was inserted subcutaneously 3-5 cm away, on the ulnar side of the  
353 recording/stimulating electrode, and a ground electrode was attached further up the  
354 participant's arm (Figure 6). The recording/stimulating electrode was advanced into  
355 the median nerve, which was located 0.3-1 cm below the skin surface. The  
356 preamplifier was taped to the participant's arm, and the acquisition hardware and  
357 stimulator were located at the outer edge of the scanner room (Figure 6). Differential  
358 responses were amplified (x10,000) using a preamplifier (NeuroAmpEX;  
359 ADInstruments, Castle Hill, Australia), band-pass filtered (0.3-5 kHz) and sampled at  
360 10 kHz using PowerLab hardware and LabChart 7 software (ADInstruments, Castle  
361 Hill, Australia).

362 The microneurographer delivered light, stroking touch to the palm to evoke  
363 activity in low-threshold mechanoreceptive afferents. A loudspeaker in the scanner  
364 room allowed the microneurographer to hear the nerve activity and a projector  
365 displayed the recording onto the scanner exterior for visual inspection. The  
366 microneurographer systematically searched for the nerve until modulations of the  
367 signal from the electrode corresponded to mass activity from mechanoreceptive  
368 afferents as a result of touch were heard. Using fine adjustments, the electrode was  
369 manipulated within the nerve to an intra-fascicular location and single units were  
370 searched for by stroking the participant's hand.

371 Single mechanoreceptive afferents were characterized by their audio and  
372 visual signals, and the extent of the receptive field of each afferent was explored  
373 using a wooden stick. The location of the receptive field was mapped using von Frey  
374 monofilaments and the minimal force required for mechanoreceptor activation noted.  
375 Afferents were identified as being myelinated A $\beta$  mechanoreceptors, namely FA1,  
376 SA1, FA2 or SA2 afferents (Vallbo & Johansson 1984). The middle of the receptive  
377 field was marked on the skin. Recordings of individual mechanoreceptive afferents in

378 response to mechanical stimulation were made (e.g. Figure 1a, b) and analyzed in  
379 MATLAB (The Mathworks; Natick, MA). Data were preprocessed to verify the single-  
380 unit nature of all recorded mechanoreceptive afferents with an offline pattern-  
381 matching algorithm.

382 **Single unit INMS:** Once a single mechanoreceptive afferent was identified, INMS  
383 was carried out to ascertain the sensation produced by a low-current electrical pulse  
384 sequence (Step 2). Trains of 30 Hz pulses (200  $\mu$ s, positive, square-wave pulses  
385 over 0.5 s) were delivered (via Stimulus Isolator; ADInstruments, Castle Hill, Australia  
386 and controlled using the LabChart 7 software). The experimenter delivered 2-3 pulse  
387 sequences, while the current was increased slowly from 0  $\mu$ A, in 1  $\mu$ A steps, until the  
388 participant felt a sensation. Once a clear sensation was felt, the precise location of  
389 the sensation and its quality were recorded and tested to confirm whether the  
390 previously mapped receptive field spatially aligned with that perceived by the  
391 participant during INMS. This was done by a process of questioning the participant to  
392 determine whether mechanical touch to the receptive field matched the projected  
393 sensory field sensation during INMS to within  $\sim$ 1 mm. If so, it was deemed that  
394 microstimulation was being applied to the afferent from which recordings had been  
395 made. If the participant felt a clear small, point-sensation in the projected sensory  
396 field that did not align with the mapped receptive field, the stimulated unit was  
397 nevertheless explored. These units were included if the perceived sensation (e.g.  
398 pressure from an SA1) was similar in quality to those in matched physiology-INMS  
399 trials (e.g. perceived size, shape, sensation) (see Table 1). The stimulating current  
400 intensity which generated a sensation was recorded, along with the stimulation  
401 currents delivered during each fMRI run. INMS of a stable, single mechanoreceptive  
402 afferent could be carried out successfully for up to  $\sim$ 45 mins, although Step 3 was  
403 completed successfully for only a subset of mechanoreceptive afferents (see  
404 Results).

405 **fMRI paradigm:** Each fMRI run consisted of a block paradigm, comprising 8 cycles  
406 of alternating periods of 8 s INMS followed by 23 s rest (acquisition time ~4 mins).  
407 The 8 s INMS period consisted of 0.5 s burst of stimulation (30 Hz pulse frequency;  
408 200  $\mu$ s pulse width) each second. For each afferent, 1-3 fMRI repeats of the INMS  
409 paradigm were conducted. In some cases, the stimulation current was adjusted  
410 between runs, e.g. due to loss of perception (Vallbo et al. 1984), to ensure a clear  
411 and stable sensation. If the INMS-induced sensation remained stable, other  
412 parameters were also tested, including changing the stimulation frequency to 60 Hz,  
413 and increasing the stimulation current to investigate the effect of recruiting further  
414 mechanoreceptive afferents (Vallbo et al. 1984).

415       After Steps 1-3, fMRI of mechanical vibrotactile stimulation at each  
416 microstimulated afferent's receptive field was carried out with identical timings to the  
417 INMS paradigm. Vibrotactile stimuli were delivered at 30 Hz to ~1 mm<sup>2</sup> of the skin  
418 using a piezo-electric device (Dancer Design, St-Helens, UK). In addition, the digit  
419 tips of each participant's left hand (and right hand for participant 4) were stimulated  
420 with 5 independently-controlled piezo-electric devices using a traveling-wave or  
421 phase-encoding paradigm (Sanchez-Panchuelo et al. 2010), analogous to that used  
422 in retinotopic mapping, in which each individual digit of the hand is sequentially  
423 stimulated to create a travelling wave of activity across cortical regions containing a  
424 somatotopic map of the hand. Vibrotactile stimulation at 30 Hz was delivered to each  
425 digit tip in periods of 4 seconds (intermittent stimulation with 0.1 s gap every 0.5 s),  
426 over a 20 s cycle. Data were collected during two runs of 12 cycles each; with  
427 stimulation delivered in a forward (digit 1 to 5) and reverse order (digit 5 to 1).

428 **fMRI acquisition:** MRI data were collected on a 7T scanner (Achieva; Philips,  
429 Amsterdam, Netherlands) using a head volume transmit coil and 32-channel receive  
430 coil (Nova Medical; Wilmington, MA). Functional data were acquired using T<sub>2</sub><sup>\*</sup>-  
431 weighted, multi-slice, single-shot gradient-echo, echo-planar imaging (EPI) with echo  
432 time (TE) 25 ms, repetition time (TR) 2000 ms, flip angle (FA) 75°, SENSE reduction



433 factor 3 in the right-left direction. The in-plane spatial resolution was 1.5 mm, field of  
434 view of  $174 \times 192 \text{ mm}^2$  in right-left and anterior-posterior directions. A slice thickness  
435 of 2.5 mm was used to achieve full brain coverage (80 mm in foot-head direction)  
436 within the TR period. For the traveling-wave paradigm, the slice thickness was  
437 reduced to 1.5 mm (48 mm coverage) as it was only necessary to span S1.

438 Following the functional runs, a high-resolution  $T_2^*$ -weighted FLASH dataset  
439 was acquired with the same slice prescription and coverage as the functional data  
440 ( $0.5 \times 0.5 \times 1.5 \text{ mm}^3$  resolution; TE/TR = 9.3/458 ms, FA =  $32^\circ$ , SENSE factor = 2),  
441 and a whole-head structural  $T_1$ -weighted MPRAGE dataset (1 mm isotropic  
442 resolution, linear phase encoding order, TE/TR 3.7/15 ms, FA  $8^\circ$ , inversion time 1184  
443 ms, TR-FOCI pulse (Hurley et al. 2010)) to allow projections of functional maps onto  
444 flattened reconstructions of the cortical space and MNI space.

445 fMRI raw time series and structural MRI scans for each subject can be found  
446 at figshare (Sanchez Panchuelo, RM; Ackerley, R; Glover, PM; Bowtell, RW;  
447 Wessberg, J; Francis, ST; McGlone, F | 2016 | fMRI to intraneural microstimulation of  
448 single mechanoreceptive afferents | Available at figshare under a CC0 Public  
449 Domain.)

450 **fMRI data analysis:** fMRI data sets were realigned to the last volume of the data set  
451 using AFNI (<http://afni.nimh.nih.gov/afni>), and statistical analysis performed using  
452 mrTools (<http://www.cns.nyu.edu/heegerlab>) in MATLAB. To account for scanner drift  
453 and other low-frequency signals, all time-series were high-pass filtered (0.01 Hz cut-  
454 off) and data converted to percent signal change. To address the key aims, three  
455 analyses were performed:

456 *Cortical responses to single unit INMS and vibrotactile stimulation in S1:* The spatial  
457 localization of microstimulated afferents in S1 was compared with digit somatotopic  
458 maps formed for each participant using a traveling-wave paradigm (Sanchez-  
459 Panchuelo et al. 2010). The somatotopic map was used to define ROIs specific to  
460 each of the 5 digits of the hand, these were subsequently used as independent ROIs

461 to allow group-level inference tests to be conducted (as performed in Besle 2013).  
462 Here, data were not spatially smoothed in order to retain high spatial resolution. Both  
463 the INMS data, and data acquired during vibrotactile stimulation applied to the skin  
464 location where each afferent was perceived, were analyzed using a general linear  
465 model (GLM) employing a canonical HRF model and its orthogonalized temporal  
466 derivative. FDR adjustment (Benjamini & Hochberg 1995) was performed using an  
467 adaptive step-up method (Benjamini et al. 2006). All adjusted P-values were  
468 converted to quantiles of standard normal distribution (Z-score). Analysis was  
469 restricted to voxels identified using the traveling-wave localizer (dilated by 5 voxels to  
470 ensure complete coverage of the S1 hand area) to reduce the number of inference  
471 tests on both the INMS and vibrotactile stimulation data to compute FDR corrected Z-  
472 scores. We investigated the spread of INMS induced activations, and vibrotactile  
473 stimulation to each unit's receptive field, by computing the mean Z-score, proportion  
474 of active voxels, and GLM parameter estimates in each digit ROI. Subsequently, to  
475 quantify spread of responses into neighboring digits at the group-level, INMS and  
476 vibrotactile responses for the ROI corresponding to the stimulated digit were  
477 combined, by averaging the mean Z-score, proportion of active voxels, and GLM  
478 parameter estimates (N=7 units; 3 Digit 1 ROIs, 2 Digit 3 ROIs, 2 Digit 4 ROIs). This  
479 procedure was then repeated for the 1<sup>st</sup> degree (N=11), 2<sup>nd</sup> degree (N=9), 3<sup>rd</sup> degree  
480 (N=5) and 4<sup>th</sup> degree (N=3) neighboring digit ROIs. A one-way analysis of variance  
481 (ANOVA) tests was then performed on this data, and post-hoc multiple pairwise  
482 comparison, adjusted for multiple comparisons using Bonferroni correction.  
483 For those units for which the stimulus sensation was lost during the fMRI run, a  
484 further GLM analysis was run which included a regressor of linear parametric  
485 modulation in time, and the associated parameter estimates were assessed.  
486 Functional statistical maps from each microstimulated afferent and the traveling-wave  
487 localizer were rendered onto flattened representations of the central sulcus obtained  
488 using the mrFlatMesh algorithm (VISTA software, <http://white.stanford.edu/software/>)

489 based on cortical segmentations from the whole head T<sub>1</sub>-weighted anatomical data  
490 obtained using Freesurfer (<http://surfer.nmr.mgh.harvard.edu/>). Having aligned  
491 functional data to the participant's whole head T<sub>1</sub>-weighted anatomical reference  
492 volume (see *Alignment of functional data*), statistical maps were transformed to  
493 flattened space using linear interpolation and displayed at the central cortical depth.  
494 *Whole brain analysis:* This was performed to compare those brain areas responding  
495 to INMS of a single mechanoreceptive afferent with those responding to vibrotactile  
496 stimulation. Data were spatially smoothed with a Gaussian FWHM 3 mm and a  
497 second GLM analysis was performed on the whole volume for both the INMS data  
498 and the vibrotactile stimulation data to the unit's receptive fields. The resulting Z-  
499 score statistical maps were threshold at  $Z < 3.08$  after FDR-adjustment and cluster-  
500 correction ( $p < 0.01$ ) to visualize activation maps and to compute binary masks for  
501 each stimulated mechanoreceptive unit (and for corresponding vibrotactile  
502 stimulation to each unit's receptive field).

503         Functional statistical maps from all five single FA1 afferents of the left hand  
504 stimulated during INMS at 30 Hz (U1, U4, U6, U8, and U11) were projected onto  
505 standard MNI space to identify active brain areas from probabilistic brain atlases  
506 (Harvard-Oxford cortical structure and Talairach Daemon labels, in FSL). Functional  
507 maps were transformed into the participant's whole head anatomical reference  
508 volume (see *Alignment of functional data*). The whole-head anatomical T<sub>1</sub>-weighted  
509 MPRAGE from each participant was aligned to a standard T<sub>1</sub>-weighted MNI template  
510 using first an affine FLIRT registration, followed by a FNIRT non-linear registration  
511 algorithm (FSL, FNIRT). This alignment was then applied to the statistical maps from  
512 the participant's INMS unit to warp the data into standard MNI space. A map was  
513 computed of the intersection of responses to all five FA1 afferents, from which to  
514 define significant regions of interest (ROIs). These ROIs were transformed to native  
515 EPI space for each individual afferent and the beta values, Z-scores and number of  
516 active voxels were interrogated for each significant ROI, in each afferent's native

517 space. Similarly, the corresponding BOLD maps resulting from vibrotactile stimulation  
518 applied to the skin location where each afferent was perceived were transformed into  
519 MNI space and identical analyses performed.

520 *Alignment of functional data to participant's whole head anatomical reference*  
521 *volume:* Statistical maps were moved from functional acquisition space into whole-  
522 head anatomical  $T_1$ -weighted space for detailed comparison with digit somatotopy in  
523 flattened reconstructions of the cortical space and for combination in standard MNI  
524 space (see *Whole brain analysis*). We estimated the alignment between the  
525 (distorted) reference EPI volume from the motion correction and the undistorted  $T_2^*$ -  
526 weighted anatomical volume using FNIRT. Functional maps were non-linearly  
527 transformed into structural  $T_2^*$ -weighted volume space using FNIRT's 'applywarp' and  
528 then linearly transformed from the structural  $T_2^*$ -weighted to whole-head  $T_1$ -weighted  
529 volume space. Note that this registration was only used for the display of statistical  
530 maps; all statistical analyses of functional data were performed in native EPI space.

531 **ACKNOWLEDGEMENTS**

532 Funding: Pain Relief Foundation grant, Medical Research Council, Vetenskapsrådet  
533 (Swedish Research Council), Royal Society International Exchanges scheme.  
534 Gratitude is extended to Professor Oleg Favorov for invaluable discussions on the  
535 manuscript.

536

537 **ABBREVIATIONS**

538	BA	Brodmann area
539	AIC	Anterior insular cortex
540	BOLD	Blood oxygenation level dependent
541	EPI	Echo-planar imaging
542	FA	Flip angle
543	FA1	Fast-adapting type 1 mechanoreceptive afferent
544	FA2	Fast-adapting type 2 mechanoreceptive afferent
545	FDR	False discovery rate
546	(f)MR(I)	(functional) magnetic resonance (imaging)
547	GLM	General linear model
548	HRF	Hemodynamic response function
549	INMS	Intra-neural microstimulation
550	M1	Primary motor cortex
551	PFC	Prefrontal cortex
552	PMC	Premotor cortex
553	PIC	Posterior insula cortex
554	PPC	Posterior parietal cortex
555	ROI	Region of interest
556	S1	Primary somatosensory cortex
557	S2	Secondary somatosensory cortex
558	SA1	Slowly-adapting type 1 mechanoreceptive afferent

559	SA2	Slowly-adapting type 2 mechanoreceptive afferent
560	SMA	Supplementary motor area
561	TE	Echo time
562	TR	Repetition time
563		
564		

565   **REFERENCES**

- 566   1.   Paul RL, Merzenich M & Goodman H (1972) Representation of slowly and  
567       rapidly adapting cutaneous mechanoreceptors of the hand in Brodmann's  
568       areas 3 and 1 of *Macaca mulatta*. *Brain Res.* 36, 229–49.
- 569   2.   Kaas J, Nelson R, Sur M, Lin C & Merzenich M (1979) Multiple  
570       representations of the body within the primary somatosensory cortex of  
571       primates. *Science* 204, 521–523.
- 572   3.   Favorov OV, Diamond ME & Whitsel BL (1987) Evidence for a mosaic  
573       representation of the body surface in area 3b of the somatic cortex of cat.  
574       *Proc. Natl. Acad. Sci. U.S.A.* 84, 6606–10.
- 575   4.   Penfield W & Boldrey E (1937) Somatic motor and sensory representation in  
576       the cerebral cortex of man as studied by electrical stimulation. *Brain* 60, 389–  
577       443.
- 578   5.   Klatzky RL, Lederman SJ & Metzger VA (1985) Identifying objects by touch:  
579       an 'expert system'. *Percept. Psychophys.* 37, 299–302.
- 580   6.   Gescheider GA, Bolanowski SJ, Pope JV & Verrillo RT (2002) A four-channel  
581       analysis of the tactile sensitivity of the fingertip: frequency selectivity, spatial  
582       summation, and temporal summation. *Somatosens. Mot. Res.* 19, 114–24.
- 583   7.   Vallbo AB & Johansson RS (1984) Properties of cutaneous mechanoreceptors  
584       in the human hand related to touch sensation. *Hum. Neurobiol.* 3, 3–14.
- 585   8.   Johansson R & Vallbo Å (1983) Tactile sensory coding in the glabrous skin of  
586       the human hand. *Trends Neurosci.* 6, 27–32.

- 587 9. McGlone, F et al. (2002) Functional neuroimaging studies of human  
588 somatosensory cortex. *Behav. Brain Res.* 135, 147–58.
- 589 10. Martuzzi R, van der Zwaag W, Farthouat J, Gruetter R & Blanke O (2014)  
590 Human finger somatotopy in areas 3b, 1, and 2: a 7T fMRI study using a  
591 natural stimulus. *Hum. Brain Mapp.* 35, 213–26.
- 592 11. Servos P, Lederman S, Wilson D & Gati J (2001) fMRI-derived cortical maps  
593 for haptic shape, texture, and hardness. *Brain Res. Cogn. Brain Res.* 12, 307–  
594 13.
- 595 12. Nelson AJ & Chen R (2008) Digit somatotopy within cortical areas of the  
596 postcentral gyrus in humans. *Cereb. Cortex* 18, 2341–51.
- 597 13. Sanchez-Panchuelo RM, Francis S, Bowtell R & Schluppeck D (2010)  
598 Mapping human somatosensory cortex in individual subjects with 7T functional  
599 MRI. *J. Neurophysiol.* 103, 2544–56.
- 600 14. Francis ST et al. (2000) fMRI of the responses to vibratory stimulation of digit  
601 tips. *Neuroimage* 11, 188–202.
- 602 15. Huang RS & Sereno MI (2007). Dodecapus: An MR-compatible system for  
603 somatosensory stimulation. *Neuroimage* 34, 1060–73.
- 604 16. Overduin SA & Servos P(2008) Symmetric sensorimotor somatotopy. *PLoS*  
605 *One* 3, e1505.
- 606 17. Blankenburg F, Ruben J, Meyer R, Schwiemann J & Villringer A (2003)  
607 Evidence for a rostral-to-caudal somatotopic organization in human primary  
608 somatosensory cortex with mirror-reversal in areas 3b and 1. *Cereb. Cortex*  
609 13, 987–93.



- 610 18. Kampe KK, Jones RA & Auer DP (2000) Frequency dependence of the  
611 functional MRI response after electrical median nerve stimulation. *Hum. Brain*  
612 *Mapp.* 9, 106–14.
- 613 19. Ferretti A et al. (2007) Cortical brain responses during passive nonpainful  
614 median nerve stimulation at low frequencies (0.5–4 Hz): an fMRI study. *Hum.*  
615 *Brain Mapp.* 28, 645–53.
- 616 20. Vallbo AB & Hagbarth KE (1968) Activity from skin mechanoreceptors  
617 recorded percutaneously in awake human subjects. *Exp. Neurol.* 21, 270–89.
- 618 21. Torebjörk HE, Vallbo ÅB & Ochoa JL (1987) Intraneural Microstimulation in  
619 Man. *Brain* 110, 1509–1529.
- 620 22. Vallbo ÅB, Olsson KÅ, Westberg KG & Clark FJ (1984) Microstimulation of  
621 single tactile afferents from the human hand. *Brain* 107, 727–749.
- 622 23. Ochoa J & Torebjörk E (1983) Sensations evoked by intraneural  
623 microstimulation of single mechanoreceptor units innervating the human hand.  
624 *J. Physiol.* 342, 633–54.
- 625 24. Kelly E, Trulsson M & Folger S (1997) Periodic microstimulation of single  
626 mechanoreceptive afferents produces frequency-following responses in  
627 human EEG. *J. Neurophysiol.* 77, 137–144.
- 628 25. Trulsson M et al. (2001) Cortical responses to single mechanoreceptive  
629 afferent microstimulation revealed with fMRI. *Neuroimage* 13, 613–22.
- 630 26. Gelnar PA, Krauss BR, Szeverenyi NM & Apkarian AV (1998) Fingertip  
631 representation in the human somatosensory cortex: an fMRI study.  
632 *Neuroimage* 7, 261–83.

- 633 27. Sanchez-Panchuelo RM et al. (2012) Within-digit functional parcellation of  
634 Brodmann areas of the human primary somatosensory cortex using functional  
635 magnetic resonance imaging at 7Tesla. *J. Neurosci.* 32, 15815–22.
- 636 28. Gati JS, Menon RS, Ugurbil K & Rutt BK (1997) Experimental determination of  
637 the BOLD field strength dependence in vessels and tissue. *Magn. Reson.*  
638 *Med.* 38, 296–302.
- 639 29. Johansson RS & Vallbo AB (1979) Tactile sensibility in the human hand:  
640 relative and absolute densities of four types of mechanoreceptive units in  
641 glabrous skin. *J. Physiol.* 286, 283–300.
- 642 30. Bianciardi M, Fukunaga M, van Gelderen P, de Zwart J & Duyn J (2011)  
643 Negative BOLD-fMRI signals in large cerebral veins. *J Cereb. Blood Flow*  
644 *Metab.* 31, 401–12.
- 645 31. Uğurbil K, Toth L & Kim DS (2003) How accurate is magnetic resonance  
646 imaging of brain function? *Trends Neurosci.* 26, 108–14.
- 647 32. Besle J, Sánchez-Panchuelo RM, Bowtell R, Francis S & Schluppeck D (2013)  
648 Single-subject fMRI mapping at 7T of the representation of fingertips in S1: a  
649 comparison of event-related and phase-encoding designs. *J. Neurophysiol.*  
650 109, 2293–305.
- 651 33. Ackerley R et al. (2012) An fMRI study on cortical responses during active  
652 self-touch and passive touch from others. *Front. Behav. Neurosci.* 6, 51.
- 653 34. Preusser S et al. (2014) The perception of touch and the ventral  
654 somatosensory pathway. *Brain.*

- 655 35. Burton H, Sinclair RJ & McLaren DG (2008) Cortical network for vibrotactile  
656 attention: a fMRI study. *Hum. Brain Mapp.* 29, 207–21.
- 657 36. Tommerdahl M, Favorov OV & Whitsel BL (2010) Dynamic representations of  
658 the somatosensory cortex. *Neurosci. Biobehav. Rev.* 34, 160–70.
- 659 37. Vickery RM, Gynther BD & Rowe MJ (1994) Synaptic transmission between  
660 single slowly adapting type I fibres and their cuneate target neurones in cat. *J.*  
661 *Physiol.* 474, 379–92.
- 662 38. Rausell E & Jones EG (1995) Extent of intracortical arborization of  
663 thalamocortical axons as a determinant of representational plasticity in  
664 monkey somatic sensory cortex. *J. Neurosci.* 15, 4270–88.
- 665 39. Landry P, Diadori P, Leclerc S & Dykes RW (1987) Morphological and  
666 electrophysiological characteristics of somatosensory thalamocortical axons  
667 studied with intra-axonal staining and recording in the cat. *Exp. brain Res.* 65,  
668 317–30.
- 669 40. Burton H & Fabri M (1995) Ipsilateral intracortical connections of  
670 physiologically defined cutaneous representations in areas 3b and 1 of  
671 macaque monkeys: projections in the vicinity of the central sulcus. *J. Comp.*  
672 *Neurol.* 355, 508–38.
- 673 41. Reed JL et al. (2010) Modular processing in the hand representation of  
674 primate primary somatosensory cortex coexists with widespread activation. *J.*  
675 *Neurophysiol.* 104, 3136–45.
- 676 42. Masamoto K, Fukuda M, Vazquez A & Kim SG (2009) Dose-dependent effect  
677 of isoflurane on neurovascular coupling in rat cerebral cortex. *Eur. J. Neurosci.*  
678 30, 242–50.

- 679 43. Hurley AC. (2010) Tailored RF pulse for magnetization inversion at ultrahigh  
680 field. *Magn. Reson. Med.* 63, 51–8.
- 681 44. Benjamini Y & Hochberg Y (1995) Controlling the false discovery rate: a  
682 practical and powerful approach to multiple testing. *J. R. Stat. Soc. Ser. B* 57,  
683 289–300.
- 684 45. Benjamini Y, Krieger A & Yekutieli D (2006) Adaptive linear step-up  
685 procedures that control the false discovery rate. *Biometrika* 93, 491–507.
- 686  
687  
688

689 **Figure legends**

690

691 **Figure 1: Physiological recordings from mechanoreceptive afferents and the**  
692 **location of afferents that were microstimulated during 7T fMRI.**

693 Example microneurography recording (top) along with the instantaneous firing  
694 frequency (bottom) for (a) an FA1 afferent (U1; see Table 1) and (b) an SA1 afferent  
695 collected inside the 7T MR scanner environment. In (a), mechanical taps were  
696 delivered to the center of the FA1's receptive field and (b) a long-lasting mechanical  
697 indentation was applied at the center of the SA1's receptive field, using a wooden  
698 stick (see gray blocks). (c) Location of the afferents that were microstimulated during  
699 7T fMRI (see Table 1). U9 was located on the right hand, but has been transposed  
700 onto the left hand for this schematic. The 'undefined' (x) afferent relates to a  
701 sensation that was felt as a line, which likely indicates two single afferents in close  
702 proximity being stimulated simultaneously.

703

704 **Figure 2: Spatial localization of INMS-induced versus vibrotactile-induced**  
705 **responses in contralateral S1.**

706

707 Activation maps related to stimulation of two different afferents in Participant 4 are  
708 rendered onto a flattened cortical patch spanning the central sulcus of the right (left  
709 of figure) and left (right of figure) hemispheres. Dark gray represents the sulci and  
710 light gray the gyri. (a) Digit somatotopy, where phase values (in radians) and  
711 corresponding preferred stimulus location (fingertip) are shown. Orderly  
712 representation of the digits is found on the posterior bank of the central sulcus (white  
713 line) and the post-central gyrus (dashed black line), corresponding to S1. (b)  
714 Statistical maps ( $Z > 3.08$ , FDR-adjusted) from INMS of U11 (left) and U9 (right).  
715 BOLD activation is localized within the expected digit ROI identified from digit  
716 somatotopy, as shown by the blue (digit 4) and red (digit 1) lines, which denote  
717 phase values encoded by the blue (3.77-5.03 rad) and orange (0-1.26 rad) colors  
718 respectively. The solid black line indicates the SI hand mask (calculated by dilating

719 the somatotopy map by 5 voxels) within which FDR correction was performed. (c)  
720 Statistical maps ( $Z > 3.08$ , FDR-adjusted) for vibrotactile stimulation of the  
721 corresponding receptive fields of U11 (top) and U9 (bottom). (d) HRF estimated from  
722 the GLM analysis for INMS and vibrotactile stimulation averaged across voxels of the  
723 ROI (U10, top; U9A, bottom). Error bars show voxel-wise parameter standard errors  
724 averaged across voxels of the ROI.

725  
726 **Figure 3: Spread of activation across the digit ROIs identified from the**  
727 **somatotopy.**

728 (a) Statistical maps ( $Z > 3.08$ , FDR-adjusted) from INMS of seven single units in  
729 participants 2, 3 and 4. In each case the activation map is rendered onto a flattened  
730 cortical patch spanning the central sulcus of the right hemisphere. Dark gray  
731 represents the sulci and light gray the gyri. The solid black line indicates the SI hand  
732 mask (calculated by dilating the somatotopy map by 5 voxels) within which FDR  
733 correction was performed. Activation is localized within the expected digit ROI (black  
734 line) identified from the digit somatotopy (see color legend). (b) Statistical maps ( $Z >$   
735  $3.08$ , FDR-adjusted) for vibrotactile stimulation of the corresponding receptive field of  
736 units. (c) Z-scores (FDR-corrected) of the INMS BOLD response averaged across  
737 voxels for each of the digit ROIs identified from the traveling-wave analysis. Error  
738 bars indicate standard error across voxels in ROI. (d) Proportion of voxels activated  
739 by the INMS paradigm at  $Z > 3.08$  (FDR-corrected) for each digit ROI. The source  
740 data for plots in panels (c) and (d) are available in the Figure 3 –source data 1.

742

743 **Figure 4: Group analysis (N = 7 units) of the BOLD response to INMS and**  
744 **vibrotactile stimulation of the unit's receptive field, showing the stimulated**  
745 **digit compared to the neighboring digits.**

746 (a) Z-scores (FDR-corrected) of INMS response in digit ROIs (defined from digit  
747 somatotopy) averaged across ROIs for the stimulated digit (N=7) compared to  
748 neighboring digits (1<sup>st</sup> degree neighbors, N=11; 2<sup>nd</sup> degree neighbors, N=9, 3<sup>rd</sup>

749 degree neighbors,  $N=5$ , 4<sup>th</sup> degree neighbors,  $N=3$ . The z-score for the stimulated  
750 digit was significantly different to that of neighboring digits.  $***P<0.0001$ ,  $**P<0.005$ ,  
751 statistical significance corrected for multiple comparison using Bonferroni correction  
752 (b) Proportion of voxels activated by the INMS (top) and vibrotactile (bottom)  
753 paradigm at  $Z>3.08$  (FDR-corrected) for the stimulated digit compared to the  
754 neighboring digits. Mean and standard error across ROIs. The proportion of active  
755 voxels in the stimulated digit ROI was significantly different to that of neighboring  
756 digits.  $***P<0.00005$ , statistical significance corrected for multiple comparison using  
757 Bonferroni procedure. (c) GLM parameter estimates of the INMS (top) and  
758 vibrotactile (bottom) paradigm for the stimulated digit compared to the neighboring  
759 digits. The parameter estimate in the stimulated digit ROI was significantly higher  
760 than that of neighboring digits.  $**P<0.01$ , statistical significance corrected for multiple  
761 comparison using Bonferroni procedure. For all plots (a) – (c) the mean and standard  
762 error across  $N$  measures is shown. The source data used for the ANOVA tests are  
763 available in the Figure 4 –source data 1.

764

765 **Figure 5: fMRI activation patterns and time courses in cortical areas.**

766 (a) Cortical activation patterns in MNI space. Transverse slices and surface  
767 reconstructions showing areas of activation in response to INMS (red clusters) and  
768 mechanical vibrotactile stimulation applied directly to the respective unit's receptive  
769 field (blue clusters), as well as areas of overlap (green clusters). Clusters represent  
770 common regions of significant activation from all single FA1 units on the left hand  
771 (U1, U4, U6, U8, and U11). Individual statistical maps for each afferent were  
772 thresholded at  $Z < 3.08$  after correcting for multiple comparisons (FDR) and cluster-  
773 corrected at  $p = 0.01$ , prior to forming the conjunction map. (b) BOLD time courses  
774 due to INMS for U4 in different cortical areas. Responses contralateral (right) to the  
775 hand stimulation site are shown in red and ipsilateral responses are shown in blue.

776

777 **Figure 6: Figure of the experimental setup.**

778 The PowerLab, NeuroAmp EX and ML180 stimulator were placed just inside the  
779 magnet room at a field strength not exceeding 5 mT. Placement of the interface  
780 equipment within the magnet room was preferred for safety reasons, as isolated  
781 cables connected to the participant did not then pass into the control room. The USB  
782 interface and trigger cables were passed through the radio frequency shield via a  
783 waveguide aperture. An amplifier and loudspeaker was driven from the NeuroAmp  
784 EX audio output to give audio feedback to the microneurographer. In addition, a  
785 projection of the computer screen could be viewed for visual confirmation of nerve  
786 signals. A switch was used to connect the electrodes to either the stimulator or the  
787 NeuroAmp head-stage pre-amplifier. In addition, a resistive shunt was placed across  
788 the stimulation leads to remove any build-up of charge before connecting or  
789 disconnecting the stimulator. Disconnection of the stimulator was necessary because  
790 of the high level of noise introduced when it was connected. Star-quad cable was  
791 used within the magnet environment to reduce the likelihood of induced currents due  
792 to scanner operation affecting the stimulus presentation.



793

794 **Tables**

795

796 **Table 1: mechanoreceptive afferent units in which INMS was performed during**

797 **7T fMRI.**

798 The table details the unit type and location, as well as the frequency and perception

799 of applied INMS. All units were located on the left hand unless stated.

800 \*A small line sensation is indicative of the simultaneous stimulation of two afferents

801 that are in close proximity.

802

Participant	Unit	Type	Location	Physiology	Sensation	Frequency
1	1A	FA1	Palm	Yes	Buzzing	30 Hz
2	2	FA1	Base of digit 1	Yes	Small dots	60 Hz
	3	SA1	Middle of digit 1	Yes	Pulling	30 Hz
	4	SA1	Base of digit 1	Yes	Pulling	30 Hz 60 Hz
	5	FA1	Middle of digit 1	Yes	Vibration	60 Hz
	6A	FA1	Digit 3 fingertip	No	Tapping, vibration	30 Hz 60 Hz 90 Hz
3	7	FA1	Base of digit 3	Yes	Small, round point of tingle sensation	30 Hz
	8A	FA1	Digit 3 fingertip	No	Small, round point of tingle sensation	30 Hz 60 Hz 90 Hz
4	9A	FA1	Middle of digit 1 <i>(right hand)</i>	No	Prickle, flutter	30 Hz
	10	Undefined	Digit 4 fingertip	No	Small line*	30 Hz
	11A	FA1	Middle of digit 4	No	Flutter	30 Hz

803

804

805

806

807 **Table 2: Cortical areas showing significant activation to INMS of single**  
 808 **mechanoreceptive afferents and the corresponding vibrotactile stimulation.**

809 Results show the mean and standard error across the five FA1 mechanoreceptive  
 810 afferents subject to INMS at 30 Hz and corresponding vibrotactile stimulation of the  
 811 perceived sensation, showing the number of units showing significant activation, MNI  
 812 coordinates, beta values, Z-score and number of voxels in ROI. Source files for  
 813 Table 2- source data 1 and Table-2 source data 2 contain single unit INMS and  
 814 vibrotactile stimulation results, respectively, for each of the 5 (U1, U4, U6, U8, U11)  
 815 individual units.

816

ROI	No. Units	x, y, z MNI co-ordinates	Single unit INMS			Vibrotactile stimulation		
			Beta	Z	Voxels	Beta	Z	Voxels
SI R	4	54, -12, 46	1.4±0.2	5.9±0.5	38±7	1.3±0.3	5.4±0.3	41±12
SI L	3	-52, -12, 44	1.2±0.2	5.6±0.8	20±9	1.6±0.3	5.2±0.2	19±1
BA 40 R	5	60, -22, 16	1.4±0.2	4.9±0.2	56±5	1.4±0.1	4.8±0.2	54±7
BA 40 L	4	-60, -22, 16	1.5±0.4	5.3±0.2	73±5	1.4±0.2	5.0±0.1	72±12
BA 43 R	2	60, -4, 10	1.1±0.4	5.4±0.1	45±6	1.2±0.4	4.4±0.2	30±20
BA 43 L	3	-58, -12, 14	1.0±0.4	4.8±0.3	33±8	1.7±0.3	4.2±0.2	26±11
SMA R	5	4, 0, 60	1.2±0.2	4.8±0.3	93±27	1.3±0.2	4.8±0.2	43±21
SMA L	5	-2, 0, 60	1.2±0.2	4.5±0.3	66±19	1.2±0.1	4.5±0.3	29±6
PMC R	4	54, 0, 50	0.8±0.2	4.7±0.2	36±11	1.1±0.2	5.0±0.2	46±9
PMC L	5	-52, -2, 50	1.1±0.1	5.5±0.3	37±7	1.2±0.1	4.3±0.1	20±8
M1 R	3	54, -6, 48	0.9±0.2	5.2±0.5	51±20	0.8±0.2	5.0±0.7	31±10
M1 L	2	-52, -6, 48	1.5±0.2	6.3±0.1	66±36	1.3±0.1	5.3±0.5	21±3
PIC R	5	46, -2, 10	0.8±0.2	4.2±0.2	45±12	0.8±0.2	4.7±0.2	27±3
PIC L	5	-42, -2, 10	0.8±0.1	4.4±0.2	38±14	-	-	-
AIC R	4	34, 26, 4	1.2±0.1	4.7±0.2	146±20	-	-	-
AIC L	4	-32, 26, 4	1.1±0.1	4.4±0.2	106±21	-	-	-
PPC R	4	38, -48, 50	1.2±0.1	4.4±0.3	168±44	-	-	-
PPC L	5	-38, -48, 56	1.0±0.1	4.4±0.3	172±43	-	-	-
PFC R	4	42, 34, 18	1.2±0.2	4.5±0.3	78±22	-	-	-

817

818

819 **Figure Supplements**

820

821 **Figure 3- figure supplement 1.**

822 **Comparison of contralateral S1 responses to different paradigms for**  
823 **Participant 1.**

824 Statistical maps overlaid on a high resolution  $T_2^*$ -weighted structural image. (a) Digit  
825 somatotopic maps obtained with the traveling-wave paradigm for both hands,  
826 showing the location of the maps in the posterior bank of the central sulcus. (b) Map  
827 of veins identified using  $T_2^*$ -weighted magnitude and phase images. Phase images  
828 are unwrapped and high-pass filtered. A map of veins is approximated by  
829 thresholding the unwrapped, filtered phase image and convolving the identified  
830 voxels with a 2 mm kernel. (c) Statistical maps ( $Z > 3.08$ , FDR-adjusted) for INMS of  
831 U1. Note, there is no activation in the S1 hand area, as shown by the ROIs  
832 delineating each of the digits. (d) Time series of the BOLD response to INMS of U1  
833 for the digit 2 ROI, denoted by the green line in image (upper panel) and of a region  
834 of activation co-localized with a vein as indicated by the white circle (lower panel).

835

836

837

838

839

840

841

842

843

844

845

846

847 **Source data**

848

849 **Table 2- source data 1.**

850 **Source files for single unit INMS.**

851 This matlab file contains 2D-matrices (19x5) with the results for single unit INMS for  
852 each of the 5 individual units (U1, U4, U6, U8, U11) in each of the 19 ROIs.

853 'BetaValues' contains mean across voxels of the beta values, 'Z-score' contains the  
854 mean Z\_score (FDR- corrected) across voxels and 'NumberVoxels' contains the  
855 number of significant active voxels ( $Z > 3.08$ , FDR-corrected) in the ROI. Table 2  
856 summarizes the results by showing the mean and standard error across the 5 units.

857

858 **Table 2- source data 2.**

859 **Source files for vibrotactile stimulation.**

860 This matlab file contains 2D-matrices (19 ROIs x 5 units) with the results for  
861 vibrotactile stimulation applied to the receptive field for each of the 5 individual units  
862 (U1, U4, U6, U8, U11) in each ROI. 'BetaValues' contains mean across voxels of the  
863 beta values, 'Z\_score' contains the mean Z-score (FDR- corrected) across voxels  
864 and 'NumberVoxels' contains the number of significant active voxels ( $Z > 3.08$ , FDR-  
865 corrected) in the ROI. Table 2 summarizes the results by showing the mean and  
866 standard error across the 5 units.

867

868 **Figure 3- source data 1.**

869 **Source files for plots of Z-score and Proportion of active voxels in each Digit**  
870 **ROI.**

871 This matlab file contains variables for each individual unit (U4, U5, U6, U8, U9, U11)  
872 with fields 'micro\_stats' and 'vibro\_stats' containing a structure with the results for  
873 single unit INMS and vibrotactile stimulation of the unit's receptive field, respectively.

874 Each structure has the following fields: 'zetaMean', 'betaSem': (5 digits x 1)-vector

875 containing mean Z-score (FDR-corrected) and standard error across voxels for each  
876 Digit ROI; 'PropActVox': (5 digits x 1)-vector containing proportion of active voxels  
877 ( $Z > 3.08$ , FDR-corrected) in each Digit ROI; and 'betaMean', 'betaSem': (5 digits x 1)-  
878 vector containing mean GLM parameter estimate and standard error across voxels  
879 for each Digit ROI. GLM parameter estimates are not plot in Figure 3 but are used for  
880 subsequent group analysis.

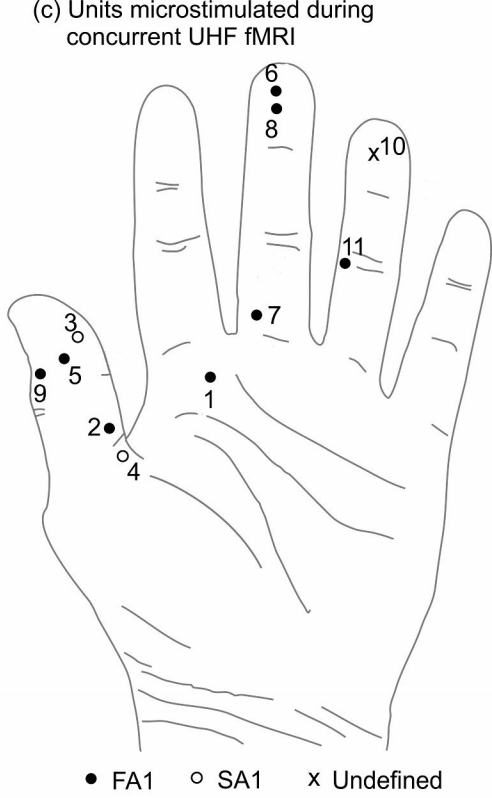
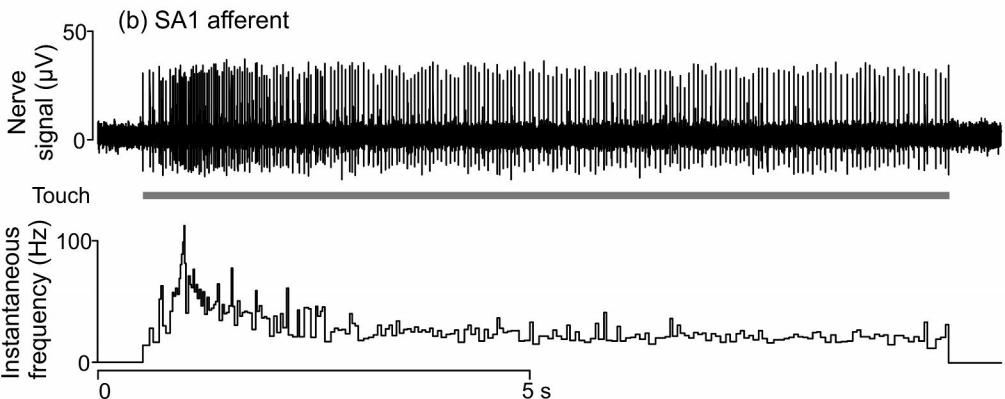
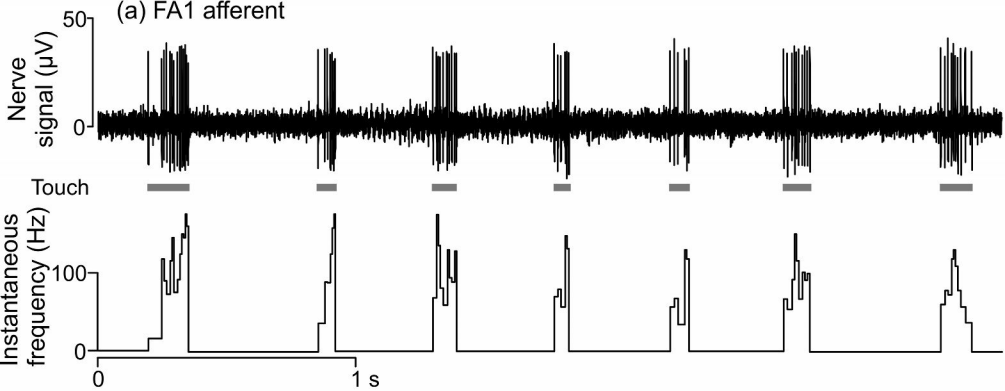
881

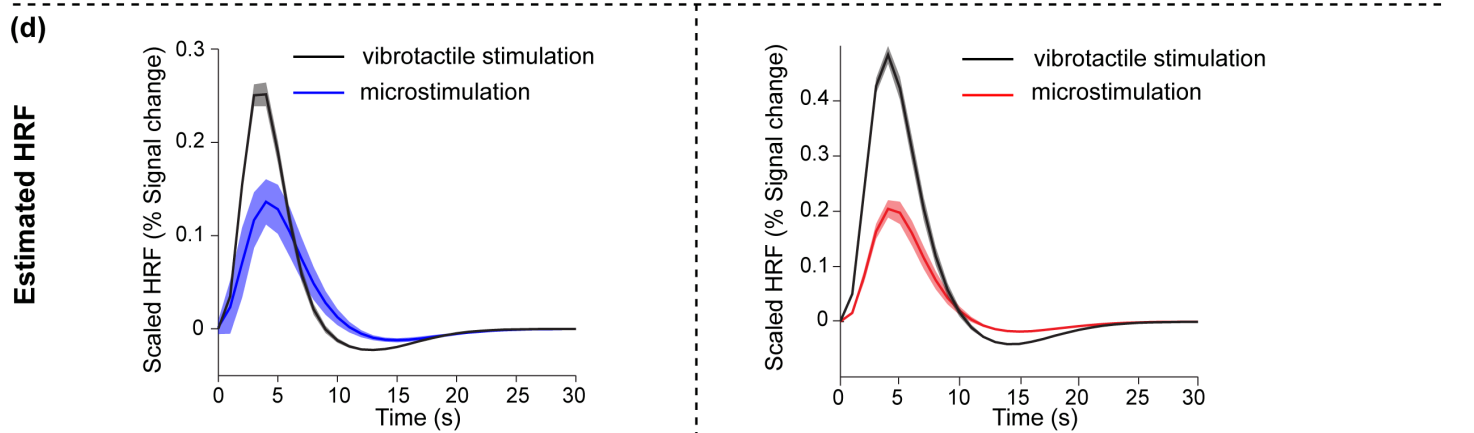
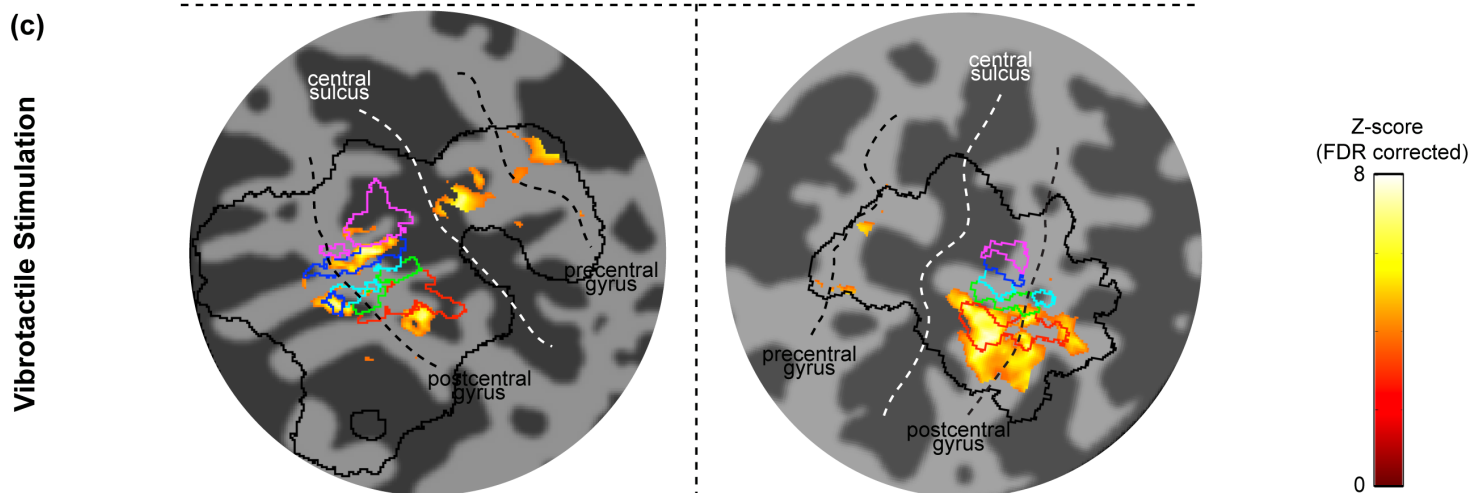
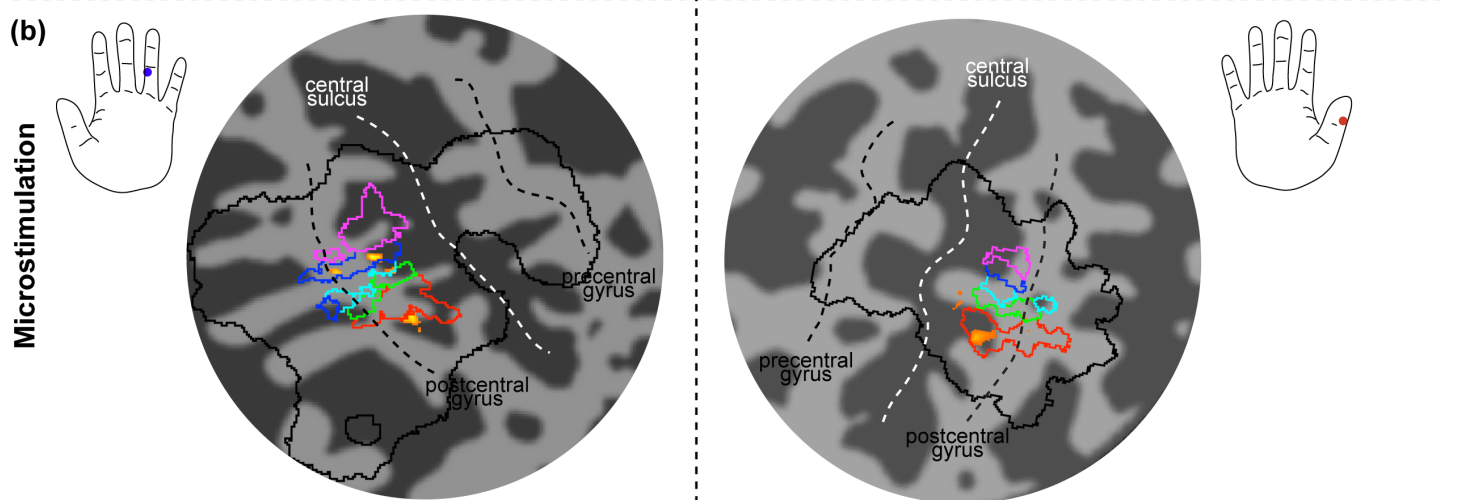
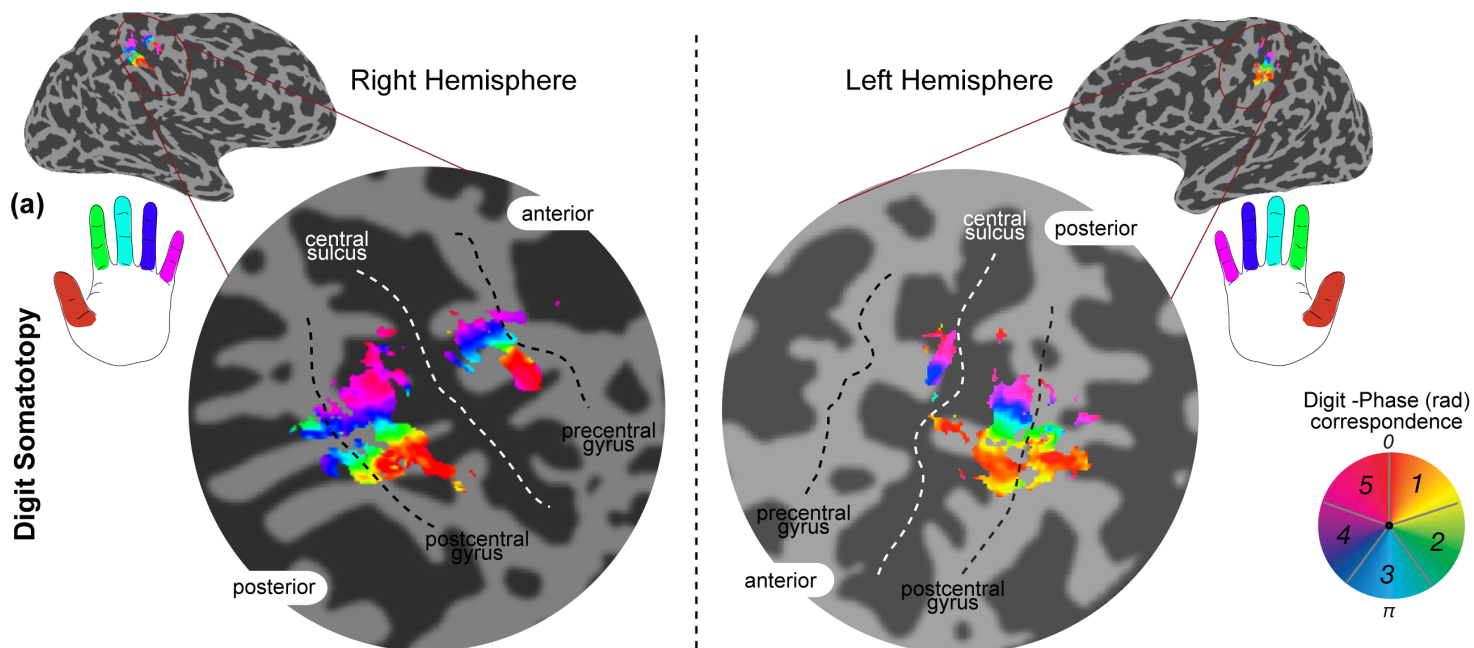
882 **Figure 4- source data 1.**

883 **Source files for ANOVA tests.**

884 This matlab file contains the 2D-matrices (11 x 5), related to each panel in Figure 4,  
885 that were used for the 1-way analysis of variance (performed using the 'anova1'  
886 matlab command). Each matrix row contains data for each of the 7 units (there are  
887 up to eleven 1<sup>st</sup> degree neighboring digit ROIs) and each matrix columns represents  
888 the 'proximity' to the stimulated digit ROI (stimulated digit ROI, 1<sup>st</sup> degree, 2<sup>nd</sup>  
889 degree, 3<sup>rd</sup> degree and 4<sup>th</sup> degree neighboring digit ROIs). 'Zeta\_micro' and  
890 'Zeta\_vibro' are the matrices containing the Z-score (FDR-corrected) values,  
891 'PerVox\_micro' and 'PerVox\_vibro' contain the proportion of active voxels ( $Z > 3.08$ ,  
892 FDR-corrected) and 'Beta\_micro' and 'Beta\_vibro' contain the GLM parameter  
893 estimates for INMS and vibrotactile stimulation respectively. ANOVA results show a  
894 significant difference in mean Z-score ( $F_{4,30}=14.08$ ,  $P < 10^{-5}$ ;  $F_{4,30}=12.97$ ,  $P < 10^{-5}$ ),  
895 proportion of active voxels ( $F_{4,30}=16.12$ ,  $P < 10^{-6}$ ;  $F_{4,30}=17.64$ ,  $P < 10^{-6}$ ) and GLM  
896 parameter estimates ( $F_{4,30}=13.52$ ,  $P < 10^{-5}$ ;  $F_{4,30}=14.1$ ,  $P < 10^{-5}$ ) across the stimulated  
897 and neighboring digit classification (INMS; vibrotactile).

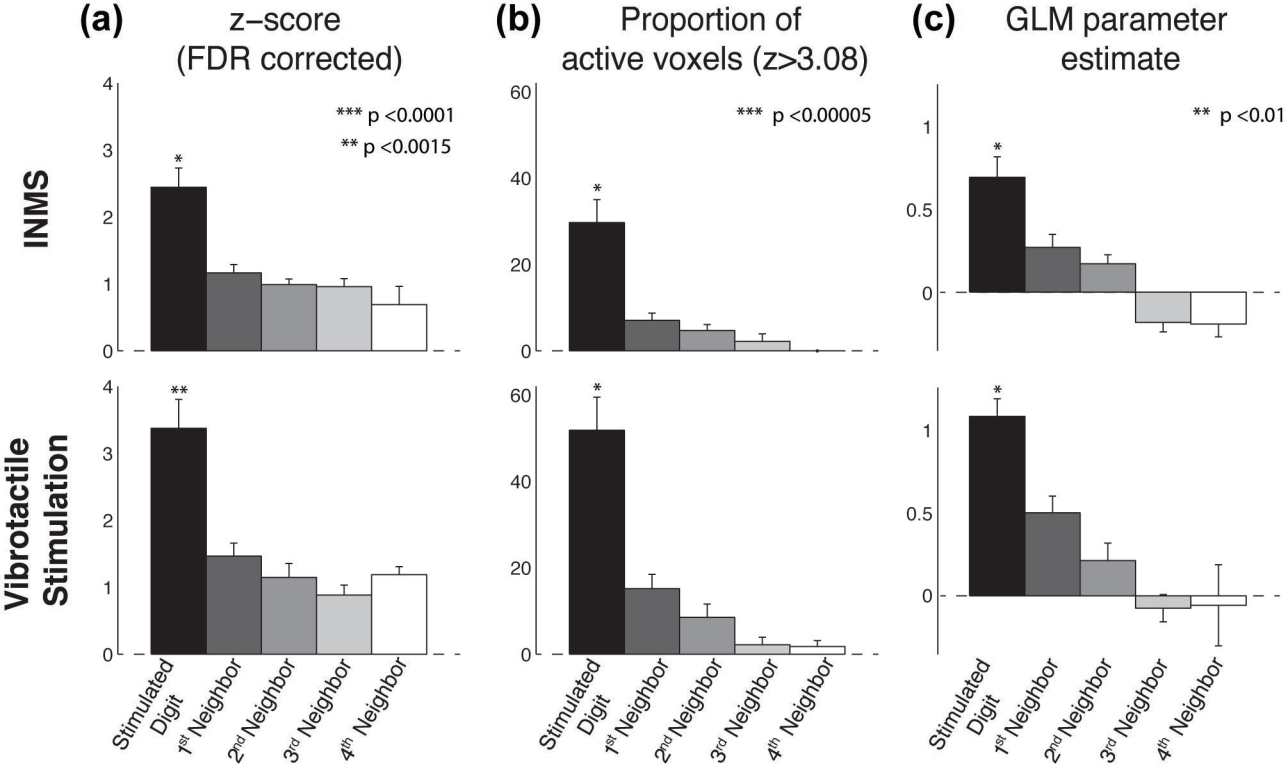
898

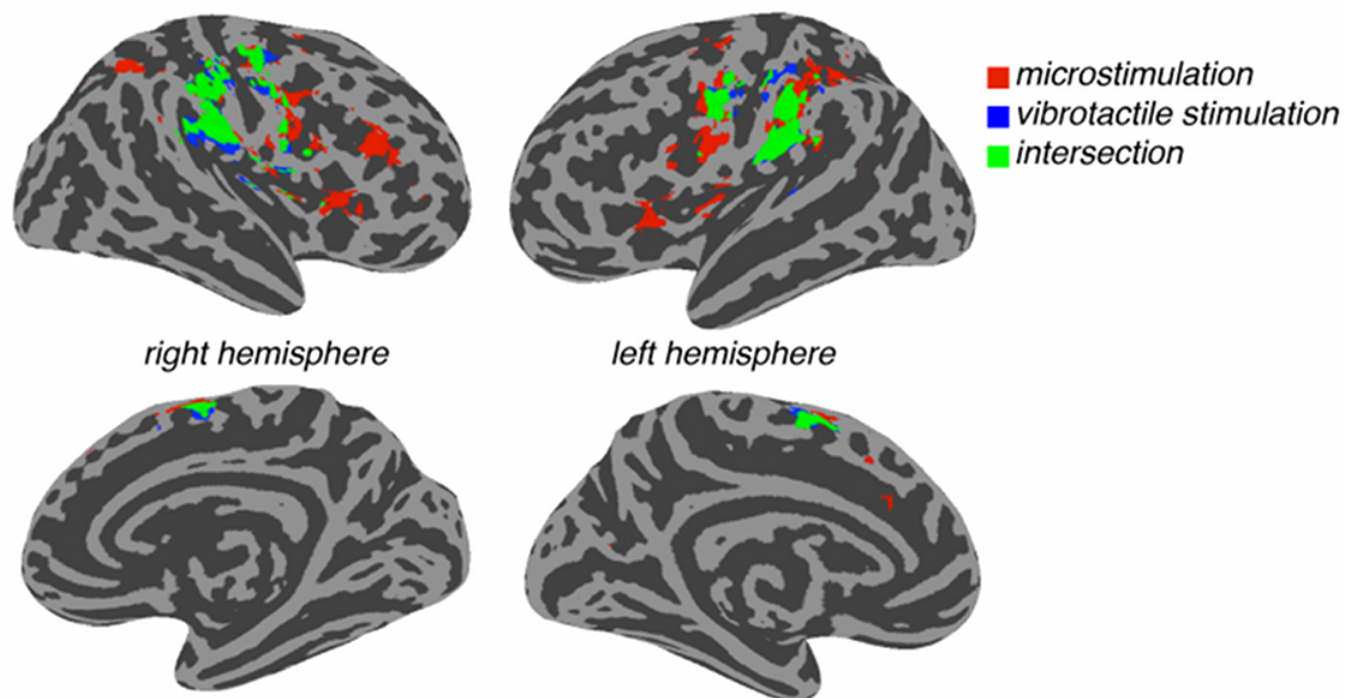
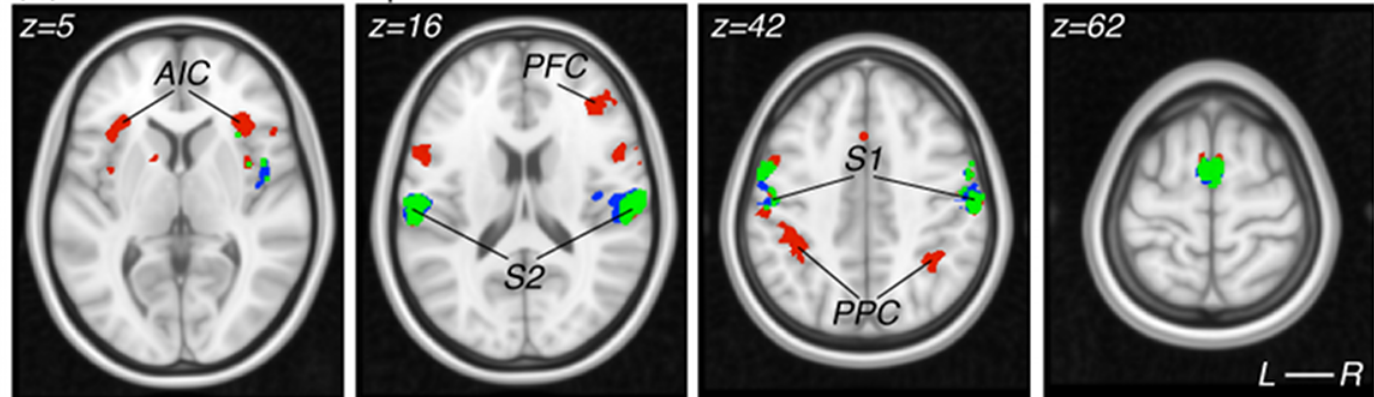
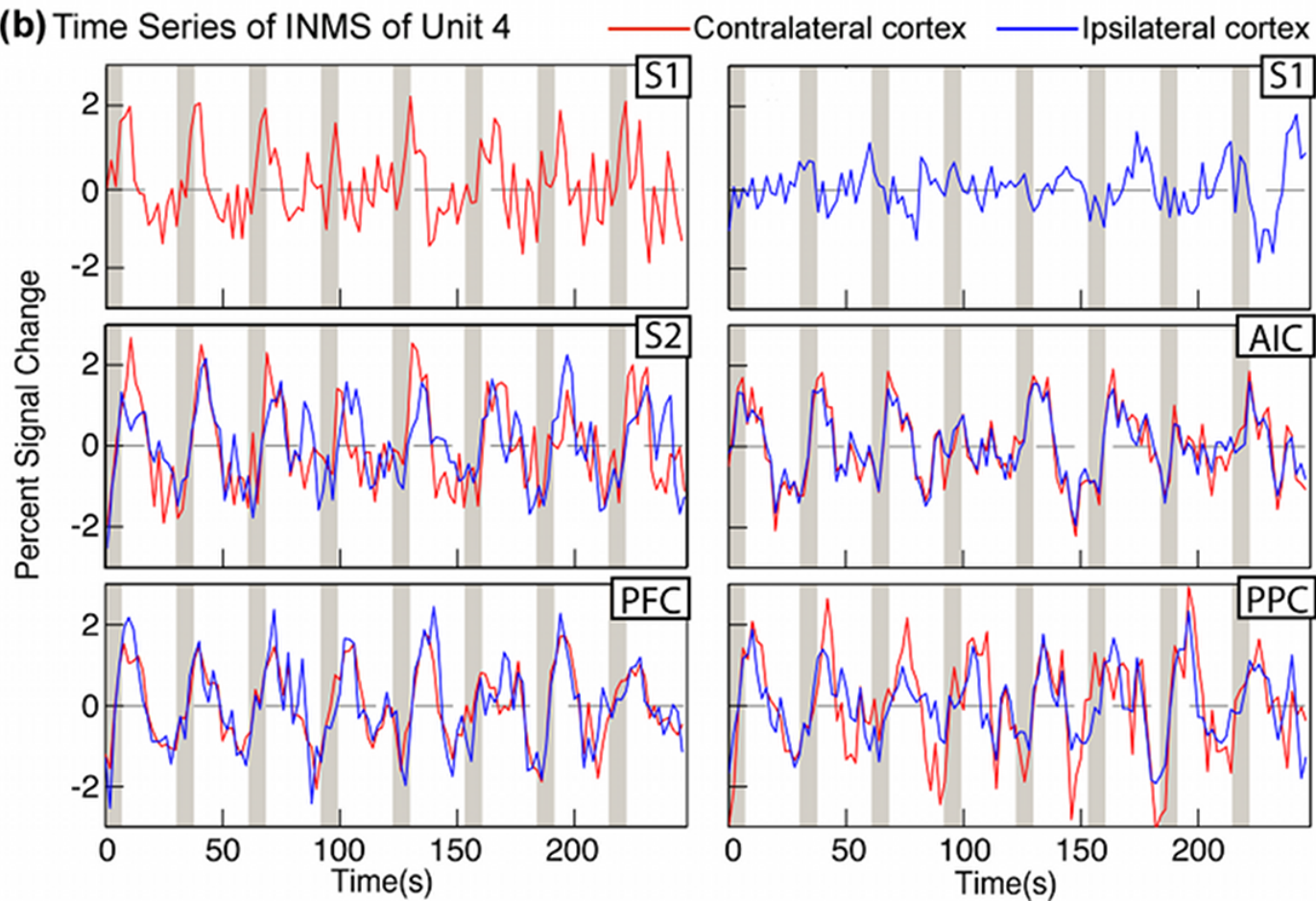




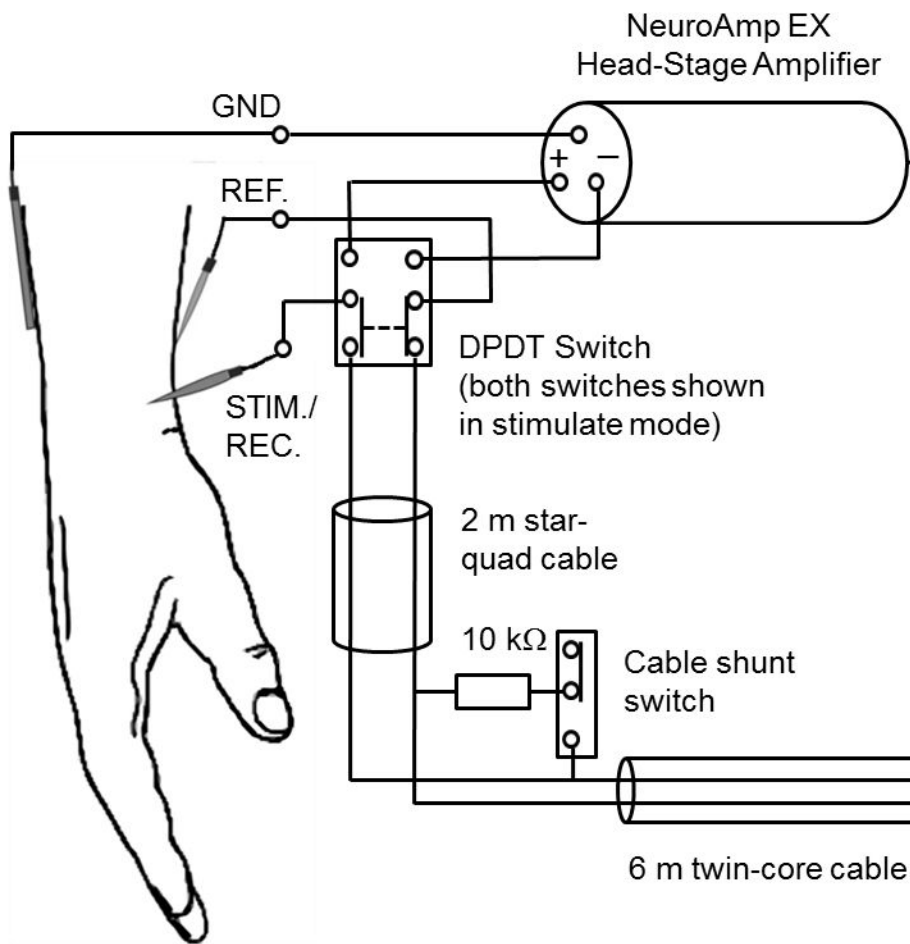




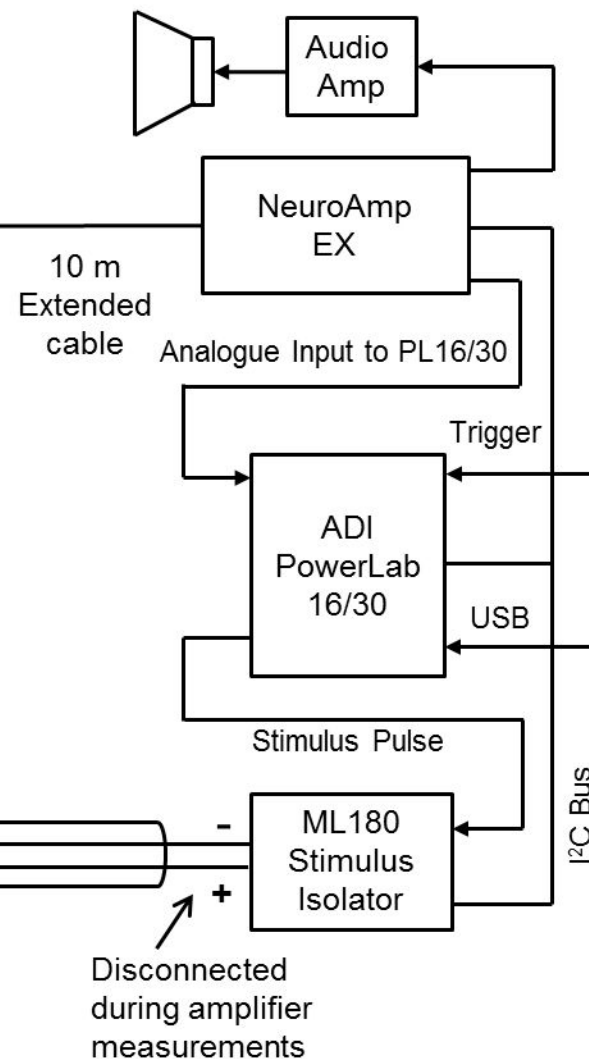


**(a) Activations in MNI space****(b) Time Series of INMS of Unit 4**

## 7 Tesla Magnet Environment



## Magnet Room (< 5 mT)



## Control Room

